Available online at www.sciencedirect.com

ScienceDirect

Journal of Ocean Engineering and Science 3 (2018) 144–155

www.elsevier.com/locate/joes

Original Article

Nonstationary fuzzy forecasting of wind and wave climate in very long-term scales

Ch.N. Stefanakos[a,*], E. Vanem[b]

[a] SINTEF Ocean, Department of Energy and Transport, Postboks 4762 Torgarden, Trondheim NO-7465, Norway
[b] DNV GL, Group Technology and Research, P.O Box 300, 1322, Høvik, Norway

Received 6 November 2017; received in revised form 12 February 2018; accepted 13 April 2018
Available online 19 April 2018

Abstract

Global climate change may have serious impact on human activities in coastal and other areas. Climate change may affect the degree of storminess and, hence, change the wind-driven ocean wave climate. This may affect the risks associated with maritime activities such as shipping and offshore oil and gas. So, there is a recognized need to understand better how climate change will affect such processes. Typically, such understanding comes from future projections of the wind and wave climate from numerical climate models and from the stochastic modelling of such projections. This work investigates the applicability of a recently proposed nonstationary fuzzy modelling to wind and wave climatic simulations. According to this, fuzzy inference models (FIS) are coupled with nonstationary time series modelling, providing us with less biased climatic estimates. Two long-term datasets for an area in the North Atlantic Ocean are used in the present study, namely NORA10 (57 years) and ExWaCli (30 years in the present and 30 years in the future). Two distinct experiments have been performed to simulate future values of the time series in a climatic scale. The assessment of the simulations by means of the actual values kept for comparison purposes gives very good results.

Keywords: Fuzzy time series; Wind and wave data; Forecasting; Nonstationary; Ocean wind and wave climate.

1. Introduction

In recent years it has become increasingly evident that the climate is changing [1]. This fact, in turn, influences the ocean wave climate, which is of great importance for the design and operation of ships and marine structures. Thus, knowledge and experience about the environmental forces and how to handle them must be supplemented with simulations of how the future climate will be. In particular, when structures are designed with an expected operational lifetime of several decades, the potential changes in the operating conditions due to climate change must be taken into account in the design stage of the structure.

Thus, there is an increasing need for very long-term wind and wave data, as climate projections require a baseline climatology against which to compare, especially in future climate scenarios produced by coupled models. Third generation spectral wave models [2,3] have been used for generating such kinds of reanalysis data sets [4–6]. See also [7], where a number of climatologies based on regional models are cited. A thorough review of wave climate hindcasts and future projections is given in [8]. A more recent review on North Atlantic storminess [9] found that most model and reanalysis studies agree on an increasing trend over the last 40–60 years, but that measured data over the last 100 years shows no general trend in the overall storminess, although they conclude that there may be an intensification of storms in the future climate.

In the present study, NORA10 [10] and ExWaCli [11] datasets are used. Especially the latter includes a number of future wave projections obtained by running a WAM implementation [2,10] with wind forcing derived from several

* Corresponding author.
E-mail addresses: christos.stefanakos@sintef.no (Ch.N. Stefanakos), erik.vanem@dnvgl.com (E. Vanem).

https://doi.org/10.1016/j.joes.2018.04.001

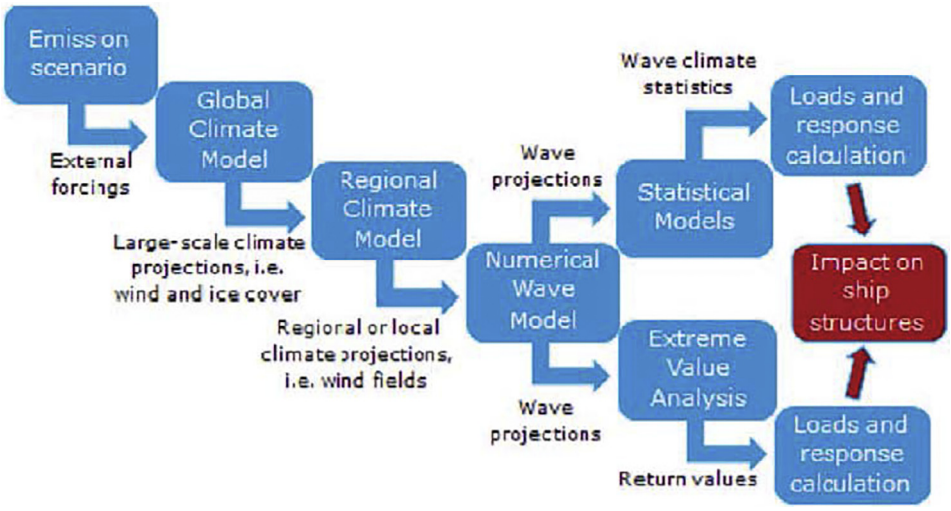

Fig. 1. Main steps in future wave climate projections (different modelling choices introduce uncertainties in each modelling step).

global circulation models [12]. A particular area in the North Atlantic Ocean is selected and the wave model has been run, in each case, for a 30-year historical period (1971–2000) and for a future period (2071–2100) assuming two different future climate scenarios, i.e. RCP 4.5 and RCP 8.5 [13,14].

There are a number of sources of uncertainties in any climate projections into the future, and future projections of the wave climate is a result of several modelling steps. Different modelling choices introduce uncertainties in each modelling step. For example, to obtain future wave climate projections, one must first run global climate models to get large-scale climate projections related to atmospheric pressures, wind fields and ice extent. However, such large-scale projections will be conditioned on projected external forcings, typically consistent with an emission scenario or a Representative Concentration Pathway (RCP). Hence, the choice of emission scenario and global climate model, as well as the initial conditions and exact parametrization of the climate model will affect the results, and are sources of uncertainties in these climate projections. Moreover, to obtain wave climate projections one typically needs higher resolution regional climate projections of wind fields, and different downscaling methods can give different results. With regional wind projections, one may use numerical wave models to obtain wave projections and there are several different wave models that may give different results. For example, in the ExWaCli project, six CMIP5 models have been selected for future wave climate projections as presented in [11]. However, the variability of climate projections from CMIP5 experiments is large, as well as the variability due to different models and model set up; see, e.g. [15] for winds, and [16,17] for waves. See also [18]. All this increase the uncertainties of future wave climate projections leading to a large variety of them. See, e.g. [19] for further discussions on the uncertainties of future wave climate projections. If one is interested in the extreme wave climate, extreme value analysis of the projected waves adds further to the overall uncertainty [20]. See also Fig. 1.

The Coupled Model Intercomparison Project Phase 5 (CMIP5) promotes a set of coordinated global climate model experiments and forms the basis for the IPCC's fifth assessment report (AR5) [1,21]. It was completed in 2014 and model output from a number of different climate models have been made available. The selection of model output to use in ExWaCli was partly pragmatic and partly based on an assessment of the individual merits of alternative models from academic work. Recently, the successor of CMIP5, CMIP6 [22], has been established, and even though there are many expectations that these data will provide a significant improvement over CMIP5 data, there are still no wave climate projections based on CMIP6 model output to date, as far as the authors are aware.

However, and because the numerical implementation of the wave models requires great computational power and high CPU time, there is an increasing interest for various soft computing techniques. Some researchers utilize Artificial Neural Networks (ANN); see, e.g. [23–27]. Some others use Fuzzy Inference Systems (FIS) in combination with Adaptive Neuro-Fuzzy Inference Systems (ANFIS); see, e.g. [28–34]. These techniques require less computational effort and they are easy to be applied.

In [35,36], FIS/ANFIS models were applied for the first time to forecast future values of the whole wave field (North Atlantic and Pacific Oceans). Usually in Fuzzy Time Series (FTS) studies, the nonstationarity is neglected. In contrast, the authors in [35–37] consider that nonstationarity should be removed from the initial time series, before starting the fuzzy forecasting procedure; especially in time series of wind and wave parameters where the nonstationary character is inherent due to the seasonal effect. So, in these works, fuzzy techniques were combined with an existing nonstationary modelling of wind and wave parameters to improve the forecasting procedure.

According to this modelling procedure, the initial nonstationary series is decomposed into a seasonal mean value, and

a residual time series multiplied by a seasonal standard deviation. The seasonal components are estimated using mean monthly values, and the residual time series is modelled as stationary series; see, e.g. [38,39]. Then, the FIS/ANFIS models are applied only to the stationary part.

In this way, the seasonal patterns, which contain all information concerning changing trends in the climate, are estimated separately from the FIS/ANFIS structure, which can be estimated by only a single point. This greatly decreases the computational time of the calculations without significant loss of the accuracy. Nonstationary modelling is finally used for the synthesis of the full simulated time series.

The present work follows the methodology presented in [35,36] but for a significantly larger forecasting horizon; namely several years. Two distinct experiments with respect to very-long (climatic) forecasting are performed based on the two datasets mentioned above. Forecasting results are compared with existing model values intentionally kept for validation of the methodology. Preliminary results of the present work has been presented in [40].

2. Methodology

2.1. Data used

Two datasets have been used for this study, as also mentioned in Introduction, namely the NORA10 and ExWaCli datasets.

The 10-km Norwegian Reanalysis (NORA10) has been developed by the Norwegian Meteorological Institute [10,41]. The atmospheric forcing is obtained by the 10-km High-Resolution Limited Area Model (HIRLAM10) [42], and the model is run nested inside a WAM model at a 50-km resolution forced by ERA-40 winds. NORA10 covers the northeast Atlantic, including the North Sea, the Norwegian Sea, and the Barents Sea.

According to [11], ExWaCli has been produced by running WAM wave model forced by winds and with ice coverage obtained from six global climate models (GFDL-CM3, EC-Earth, HADGEM2, IPS-CM5A-MR, MRI-GCGCM3 and MIROC5) by downscaling the wind fields from the climate models to a 50 km grid. The model is set up on a rotated spherical grid with approximately 50 km resolution, covering the Northeast Atlantic. See also [43].

The referred area is in the North-eastern Atlantic Ocean, west of the British Isles, and the computational domains partially overlap; see Fig. 2. At each datapoint, three-hourly time series of significant wave height, wave period and wind speed are available. The NORA10 dataset covers the period 1957.09.01–2014.08.31, i.e. approximately 57 years, while ExWaCli dataset includes a historic period of 30 years (1971–2000) and two future wave projections of 30 years for the period 2071–2100 assuming two different future climate scenarios (RCP 4.5 and RCP 8.5). The span of the datasets is depicted in Fig. 3.

Both datasets used in this study have been validated previously. A validation of NORA 10 data against measured data

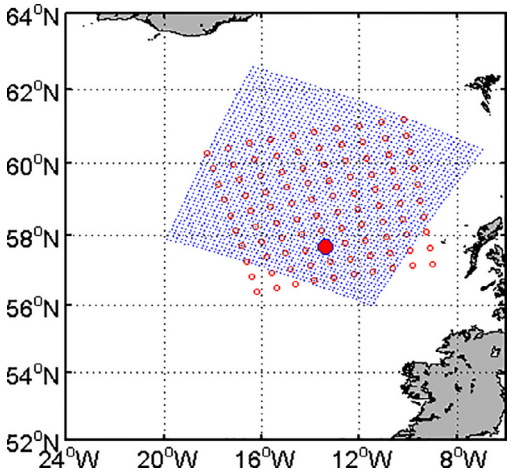

Fig. 2. Computational domains and data points used (blue: NORA10, red: ExWaCli).

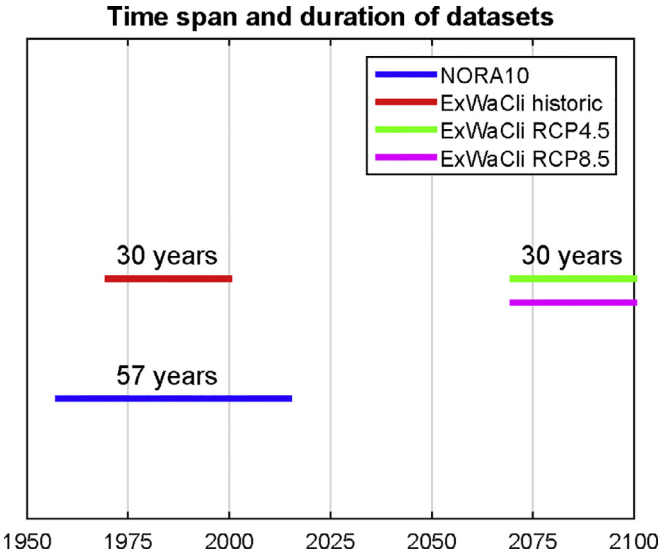

Fig. 3. Time span and duration of datasets.

was presented in [10], where the model wave data were compared to both in situ measurements and satellite observations. Compared to e.g. the ERA-40 hindcast the NORA 10 data exhibited a significant improvement in mean values and high percentiles. The near-surface wind profiles from NORA 10 were compared against measurements in [44]. A more recent comparison study of the NORA 10 wave data against measured data is presented in [45], demonstrating good agreement between NORA 10 and measured data. The NORA 10 data have generally been acknowledged to be a good dataset for the wave and wind conditions in the North Atlantic, and have been used in several independent studies on the North Atlantic wave climate, see e.g. [46,47]. The ExWaCli data have again been validated against NORA 10 data, as outlined in [11,43]. Hence, no further validation of these datasets are deemed necessary and the focus of this paper is on nonstationary fuzzy forecasting models and not in the actual data generation and validation.

2.2. Model setup

The present work closely follows the methodology described in [35,36], according to which the initial nonstationary time series of wind and wave parameters are first decomposed as follows:

$$Y(t) = m(t) + s(t)\, W(t), \tag{1}$$

where $m(t)$ and $s(t)$ are deterministic periodic functions with a period of one year, and $W(t)$ is a zero-mean, stationary, stochastic process. The functions $m(t)$ and $s(t)$ are seasonal mean value and seasonal standard deviation, respectively, and describe the exhibited seasonal patterns. The seasonal patterns (mean value and standard deviation) are obtained by means of:

$$\widetilde{\mu}_3(m) = \frac{1}{J}\sum_{j=1}^{J}\frac{1}{K_m}\sum_{k=1}^{K_m} Y(j, m, \tau_k), \tag{2}$$

$$\widetilde{\sigma}_3(m) = \frac{1}{J}\sum_{j=1}^{J}\sqrt{\frac{1}{K_m}\sum_{k=1}^{K_m}\left[Y(j, m, \tau_k) - \mu_3(j, m)\right]^2}, \tag{3}$$

with $m = 1,2,...,12$. Note that, $Y(j,\ m,\ \tau_k)$ is a re-parameterization of $Y(t)$, where j is the year index, m represents the monthly index, τ_k is the time within a month, $k = 1, 2, \ldots, K_m$, and K_m is the total number of observations within a month. In [35,48], it has been shown that, periodic extensions of quantities $\widetilde{\mu}_3(m)$ and $\widetilde{\sigma}_3(m)$ are good estimates of periodic functions $m(t)$ and $s(t)$.

In this way, the information contained in the time series $Y(t)$ is decomposed into two parts:

- one deterministic $[m(t), s(t)]$, containing information about features such as seasonal variability, interannual variability, climatic trends, and evolving more slowly in time, and
- one stochastic $[W(t)]$, containing info about the dependency (correlation) structure of the successive values of the series, and evolving more rapidly in time.

The simulation procedure is applied to the second one, as only this part has been modelled as a stochastic one. The first part (deterministic) is estimated by means of the existing values and is used in the end to reconstruct the simulated version $\widehat{Y}(t)$ of the initial nonstationary series.

Further, model (1) can be generalized in the multivariate case as follows:

$$\underset{(N\times 1)}{\mathbf{Y}(t)} = \underset{(N\times 1)}{\mathbf{M}(t)} + \underset{(N\times N)}{\mathbf{\Sigma}(t)}\ \underset{(N\times 1)}{\mathbf{W}(t)}, \tag{4}$$

where N is the number of time series. The vector $\mathbf{M}(t)$ and the matrix $\mathbf{\Sigma}(t)$ are deterministic periodic functions with a period of one year, and the vector $\mathbf{W}(t)$ is assumed to be a zero-mean, stationary, stochastic process. As in the univariate case, the functions $\mathbf{M}(t)$ and $\mathbf{\Sigma}(t)$ describe the exhibited seasonal patterns. Note that the seasonal standard deviation $s(t)$ of the univariate case has been replaced in the multivariate case by the square root of the covariance matrix, which introduces interactions among the various terms of the initial time series vector $\mathbf{Y}(t) = [Y_1(t)Y_2(t)\cdots Y_n(t)\cdots Y_N(t)]^{\mathrm{T}}$.

Representation (4) can be equally well used either for the modelling of a multivariate time series of wind and wave parameters at a specific location at sea or for the modelling of the long-term field of a wind or wave parameter. Especially in the latter case, if grid points are correlated only with some of their neighbouring points, one can reduce the interactions by keeping only those interactions as follows:

$$\underset{(N\times 1)}{\mathbf{Y}(t)} = \underset{(N\times 1)}{\mathbf{M}(t)} + \underset{(N\times N)}{\mathbf{\Sigma}(t)}\left[\underset{(N\times N)}{\mathbf{Q}(n)}\ \underset{(N\times 1)}{\mathbf{W}(t)}\right], \tag{5}$$

where $\{\mathbf{Q}(n),\ n = 1, 2, \ldots, N\}$ is a set of diagonal matrices depending on n. Thus, to each component $Y_n(t)$ of matrix $\mathbf{Y}(t)$ corresponds a different matrix $\mathbf{Q}(n)$. The diagonal of these matrices contains 1's and 0's, including in this way only those grid points that are correlated with point n.

Then, the FIS/ANFIS forecasting methodology described in [35], is applied to the stationary part $W(t)$. The membership functions to form the fuzzy input sets are simple linear functions and the FIS systems are established assuming the following IF-THEN rules:

(a) wind speed W_S:

$$W_S(t+1) = f_1\big(W_S(t)\big) = p_k^{(1)} W_S(t) + s_k^{(1)}, \tag{6}$$

(b) significant wave height H_S:

$$H_S(t+1) = f_2\big(W_S(t), H_S(t)\big) = p_k^{(2)} W_S(t) + q_k^{(2)} H_S(t) + s_k^{(2)}, \tag{7}$$

where the parameters $\left\{p_k^{(\cdot)}, q_k^{(\cdot)}, s_k^{(\cdot)}\right\}$ in Eqs. (6) and (7) are estimated using the ANFIS procedure.

Finally, using Eq. (1), the simulated time series $\widehat{W}(t)$ is combined with the estimated seasonal components $m(t)$ and

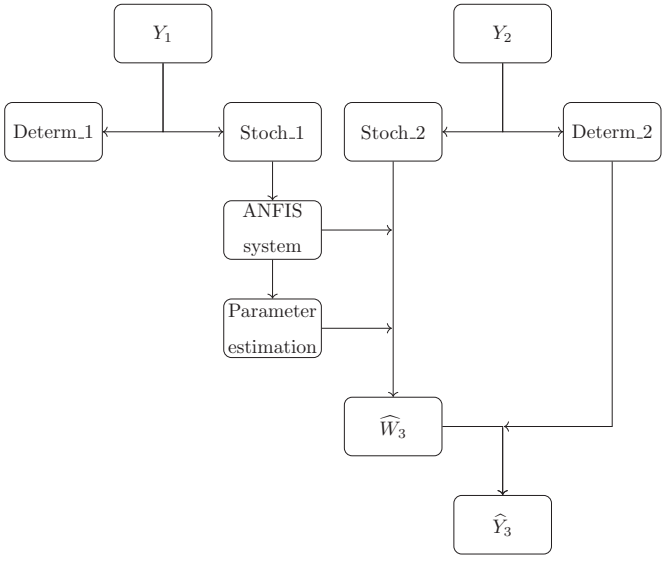

Fig. 4. Schematic of the procedure followed in the two experiments (1: training, 2: input, 3: simulated datasets).

$s(t)$ to give a simulated version $\widehat{Y}(t)$ of the initial nonstationary series.

2.3. Measuring forecasting quality

To evaluate forecasting performance, the following error measures have been used:

(a) Root Mean Square Error (RMSE) defined as

$$\mathrm{RMSE} = \sqrt{\frac{1}{I}\sum_{i=1}^{I}|e(t_i)|^2} \tag{8}$$

(b) Mean Absolute Percentage Error (MAPE) defined as

$$\mathrm{MAPE} = \frac{1}{I}\sum_{i=1}^{I}\left|\frac{e(t_i)}{a(t_i)}\right|, \tag{9}$$

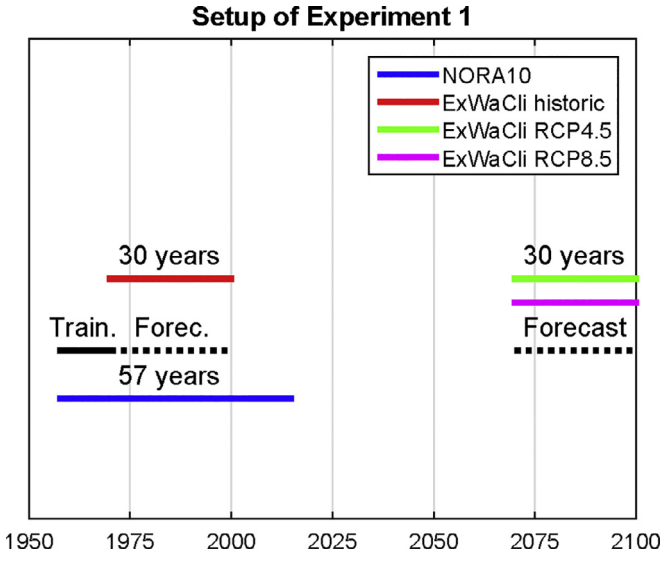

Fig. 5. Setup of Experiment 1.

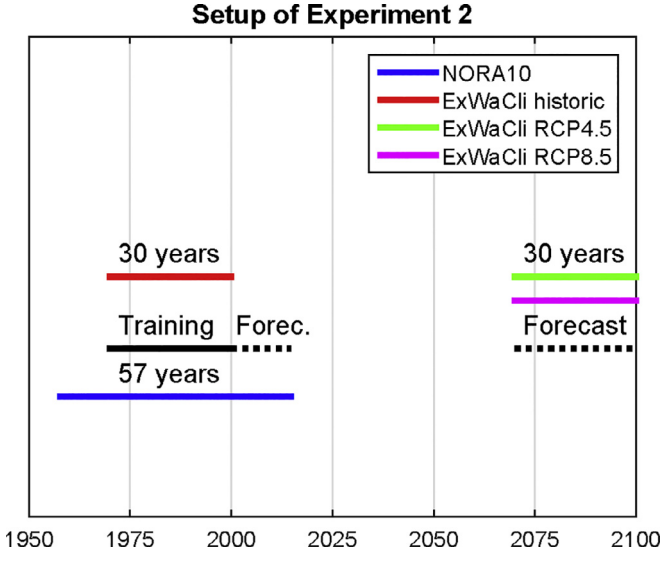

Fig. 6. Setup of Experiment 2.

where

$$e(t_i) = a(t_i) - f(t_i) \tag{10}$$

denotes the forecasting error at time t_i between forecasts $f(t)$ and actual values $a(t)$.

(c) Mean Absolute Scaled Error (MASE) defined as

$$\mathrm{MASE} = \frac{1}{I}\sum_{i=1}^{I}|q(t_i)|, \tag{11}$$

where

$$q(t_i) = \frac{e(t_i)}{\frac{1}{N}\sum_{n=2}^{N}\left|X(t_n) - X(t_{n-1})\right|}, \tag{12}$$

where $\{X(t_n),\ n = 1, 2, \ldots, N\}$ are the existing values, used for training of the fuzzy time series model.

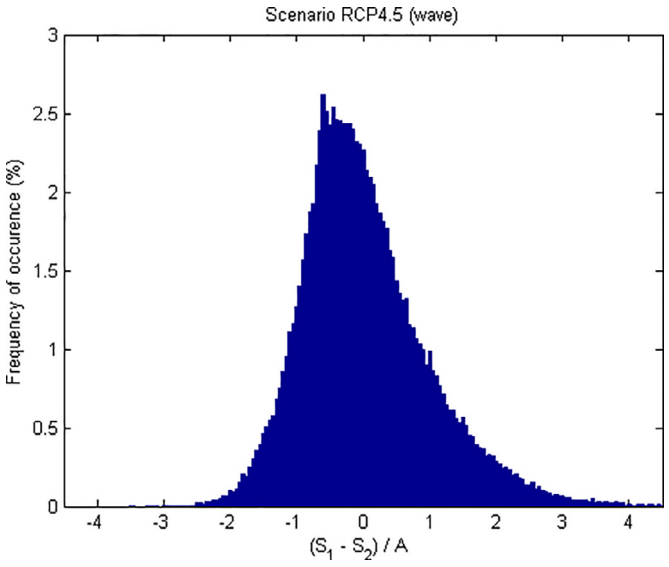

Fig. 7. Relative difference of the two estimates with respect to actual values for scenario RCP4.5 (1: Exp1, 2: Exp2, A: actual values).

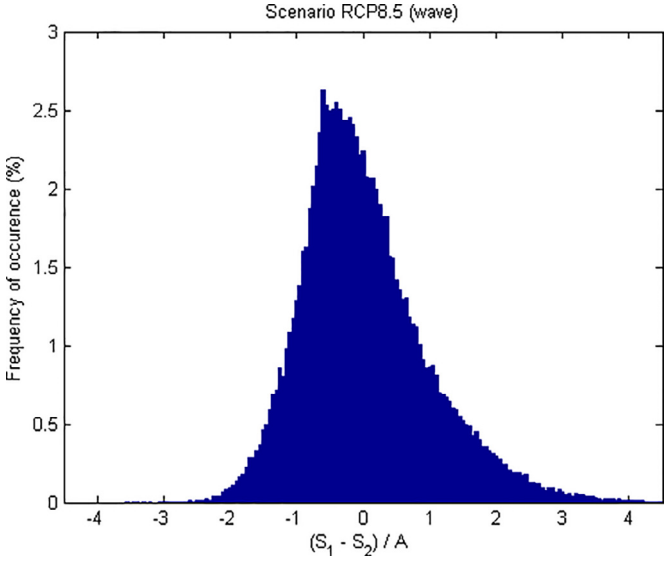

Fig. 8. Relative difference of the two estimates with respect to actual values for scenario RCP8.5 (1: Exp1, 2: Exp2, A: actual values).

(d) Root Mean Square Scaled Error (RMSSE) defined as

$$\text{RMSSE} = \sqrt{\frac{1}{I}\sum_{i=1}^{I}|q(t_i)|^2} \tag{13}$$

(e) Bias:

$$\text{Bias} = \frac{1}{I}\sum_{i=1}^{I}[-e(t_i)], \tag{14}$$

(f) Scatter Index (SI) in %:

$$\text{SI} = \sqrt{\frac{RMSE}{\sum_{i=1}^{I} a(t_i)}} \times 100, \tag{15}$$

(g) Correlation coefficient R^2:

$$R^2 = \frac{\sum_{i=1}^{I}\Big(f(t_i)-\overline{a}\Big)\Big(a(t_i)-\overline{a}\Big)}{\sqrt{\sum_{i=1}^{I}\Big(f(t_i)-\overline{a}\Big)^2 \sum_{i=1}^{I}\Big(a(t_i)-\overline{a}\Big)^2}}, \tag{16}$$

where

$$\overline{a} = \frac{1}{I}\sum_{i=1}^{I} a(t_i). \tag{17}$$

Results from all error measures are calculated and given in the next section, showing the accuracy of the proposed forecasting methodology.

3. Numerical results

First, results for a point-wise study are given in Section 3.1. Further results for the whole field are given in Section 3.2.

3.1. Point-wise results

Two points from the two datasets have been chosen with neighbouring coordinates, so that the results are directly comparable; see Fig. 2.

Two experiments have been designed. In both experiments the following simulation procedure has been applied; see also Fig. 4 where the procedure is summarized.

1. A dataset Y_1 is chosen as the Training set.
2. Decomposition (1) is applied to Y_1.
3. Residual part W_1 is used as input for the estimation of the structure and the parameters of the FIS/ANFIS system.
4. A second dataset Y_2 is chosen as the Input dataset.
5. Step 2 is applied to Y_2.

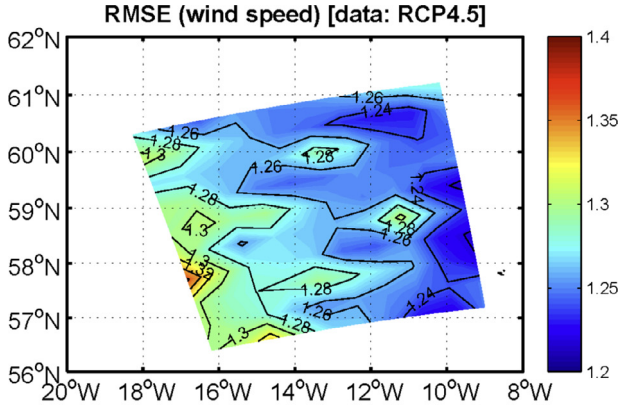

(a) RCP4.5

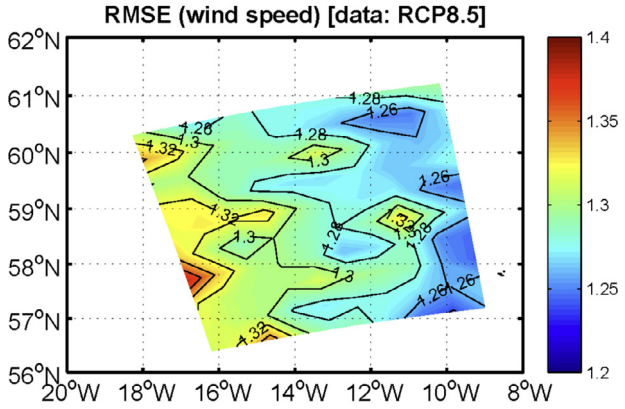

(b) RCP8.5

Fig. 9. RMSE of the wind speed estimates for Experiment 1 with respect to actual values for scenarios RCP4.5 and RCP8.5.

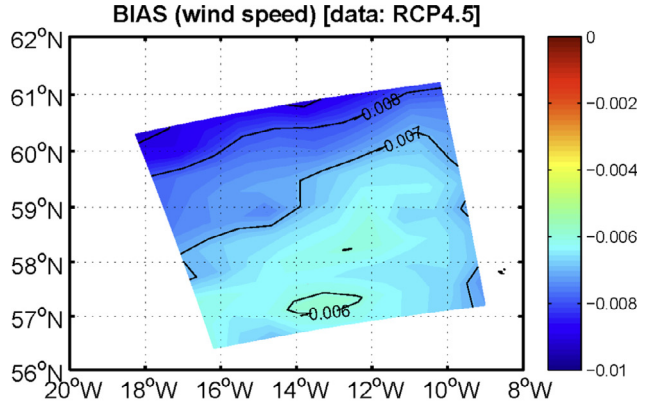

(a) RCP4.5

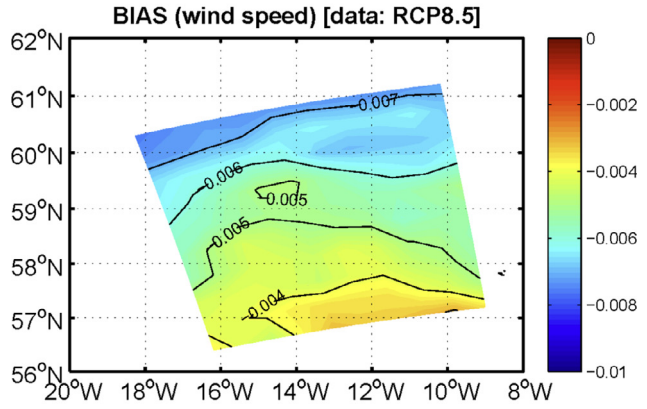

(b) RCP8.5

Fig. 10. Bias of the wind speed estimates for Experiment 1 with respect to actual values for scenarios RCP4.5 and RCP8.5.

6. Residual part W_2 is used as input for the simulation based on the FIS/ANFIS system estimated in Step 3 to get the output series $\widehat{W}_3$.
7. Series $\widehat{W}_3$ is combined with the deterministic part of Y_2 estimated in Step 5 and the final simulated time series $\widehat{Y}_3$ is obtained.

In Experiment 1, the first part of the NORA10 dataset (1957–1970) has been chosen as the Training set, based on which the FIS/ANFIS structure is estimated. Then, one simulation is obtained for the historic period (1971–2000) and two for the future one (2071–2100). See also Fig. 5 where the setup of Experiment 1 is shown. The results of the three simulations are compared with the three ExWaCli datasets (ExHist, ExR45, ExR85).

In Experiment 2, the historic part of ExWaCli dataset (1971–2000) has been chosen as the Training set for the estimation of the FIS/ANFIS structure. Then, one simulation is obtained for the historic period (2001–2014) and two for the future one (2071–2100). See also Fig. 6 where the setup of Experiment 2 is shown. The results of the three simulations are compared the first one with the last part of NORA10 dataset and the other two with the two future ExWaCli datasets (ExR45, ExR85).

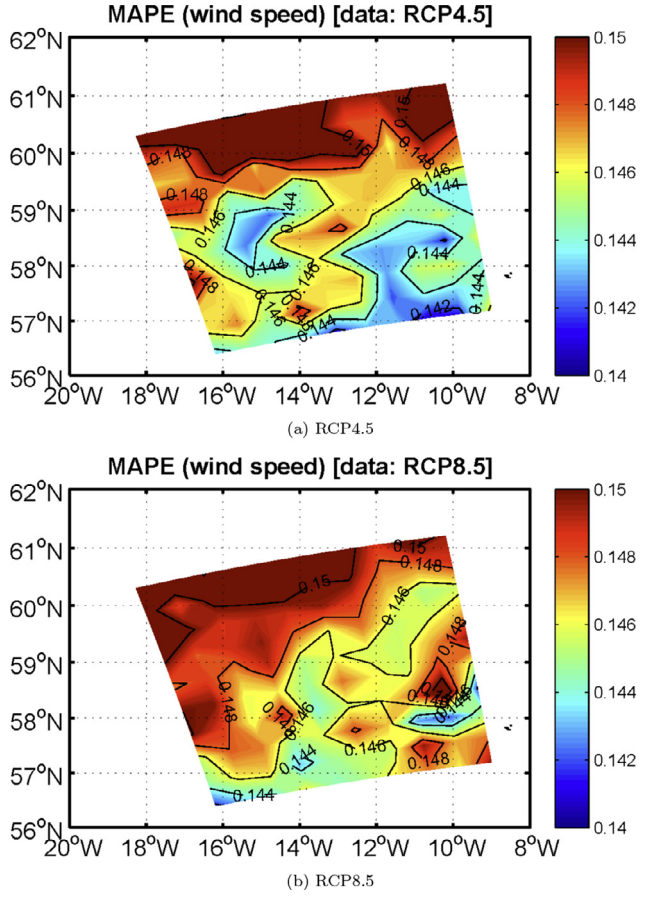

Fig. 11. MAPE of the wind speed estimates for Experiment 1 with respect to actual values for scenarios RCP4.5 and RCP8.5.

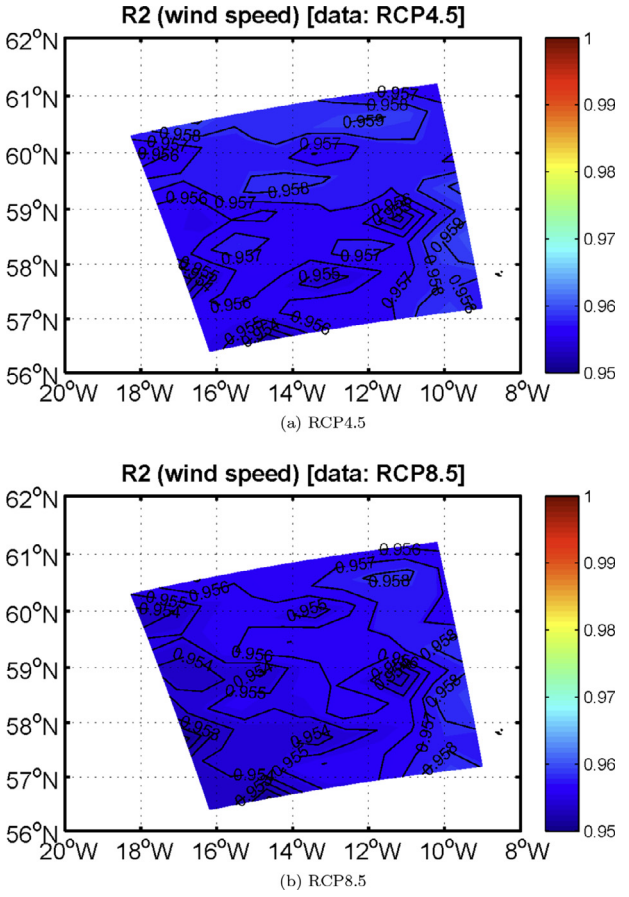

Fig. 12. R^2 of the wind speed estimates for Experiment 1 with respect to actual values for scenarios RCP4.5 and RCP8.5.

It should be stressed here that Steps 3 and 6 (forecasting part) of the aforementioned procedure are applied to the stationary part of the series $\widehat{W}$. Thus, it is of essential importance to remove the deterministic (periodic) character of the series first, namely Determ_1 and Determ_2 in Fig. 4. In this way, data from different models can be combined in the estimation process of future values, since only the probabilistic structure of the series is taken into account. All future climatic trends are included in the extracted part, which will be added again at the end of the procedure (Step 7).

In addition, although the deterministic part Determ_2 is estimated in the present work by means of the existing time series, it could have been replaced by any other relevant estimates concerning the future trends of that time period, obtained by any other appropriate climatic model.

In Tables 1 and 2, the error measures of wind speed and significant wave height, respectively, are given for Experiment 1. The corresponding measures for Experiment 2 are given in Tables 3 and 4.

In all cases, the results are very good. For example, there is a very good correlation between the simulations and the actual values of the order 91–95% (wind speed) and 98% (wave height). The bias is almost zero and the root-mean-square is of the order of magnitude of some centimetres for wave height and less than 2 m/s for wind speed. Experience

Table 1
Error measures for wind speed, Experiment 1.

Dataset	ExHist	ExR45	ExR85
RMSE	1.341	1.296	1.314
MAPE	0.154	0.147	0.146
MASE	1.003	1.002	1.003
RMSSE	1.400	1.397	1.404
R^2	0.953	0.954	0.953
SI (%)	13.715	13.512	13.643
Bias	−0.005	−0.006	−0.005

Table 2
Error measures for wave height, Experiment 1.

Dataset	ExHist	ExR45	ExR85
RMSE	0.269	0.268	0.263
MAPE	0.047	0.046	0.046
MASE	0.843	0.833	0.811
RMSSE	1.321	1.364	1.324
R^2	0.990	0.989	0.990
SI (%)	7.785	8.126	7.986
Bias	−0.003	−0.003	−0.003

Table 3
Error measures for wind speed, Experiment 2.

Dataset	ExR45	ExR85	NORA10
RMSE	1.290	1.308	1.802
MAPE	0.140	0.139	0.187
MASE	0.991	0.992	0.984
RMSSE	1.391	1.398	1.389
R^2	0.954	0.954	0.913
SI (%)	13.453	13.584	18.383
Bias	0.000	0.001	−0.002

Table 4
Error measures for wave height, Experiment 2.

Dataset	ExR45	ExR85	NORA10
RMSE	0.258	0.254	0.308
MAPE	0.046	0.045	0.057
MASE	0.826	0.808	0.865
RMSSE	1.316	1.279	1.339
R^2	0.990	0.991	0.985
SI (%)	7.836	7.714	9.142
Bias	0.001	0.001	−0.008

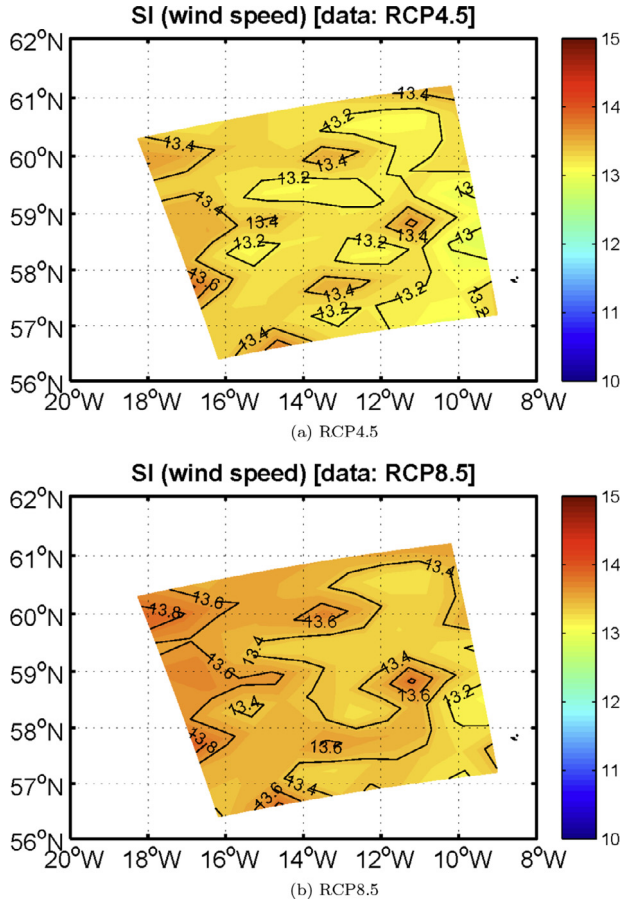

(a) RCP4.5

(b) RCP8.5

Fig. 13. SI of the wind speed estimates for Experiment 1 with respect to actual values for scenarios RCP4.5 and RCP8.5.

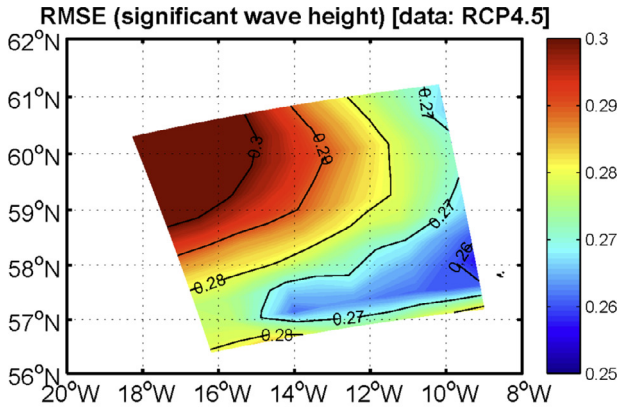

(a) RCP4.5

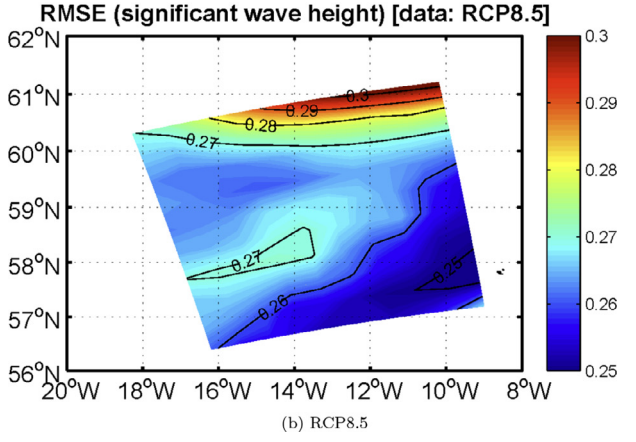

(b) RCP8.5

Fig. 14. RMSE of the wave height estimates for Experiment 1 with respect to actual values for scenarios RCP4.5 and RCP8.5.

with more data points will reveal if the slightly higher errors in the case of wind speed are significant or not.

By comparing the forecasting performance of the two experiments for the future scenarios RCP4.5 and 8.5, one can conclude that both are in a very good agreement with the actual values of the datasets, which means that either dataset (NORA10 and ExWaCli.historic) can be equally well used as a Training dataset for the estimation of the parameters of the FIS/ANFIS procedure after the appropriate deseasonalization.

As an example, the relative differences between the results from the two experiments are calculated as follows. If $S_1(t)$, $S_2(t)$ are the estimates of the two experiments, respectively, and $A(t)$ are the actual values retained for comparison, then the relative differences are defined as

$$Rdf(t) = \frac{S_1(t) - S_2(t)}{A(t)} \times 100. \tag{18}$$

In Figs. 7 and 8, the histograms of $Rdf(t)$ for H_S are shown for the two climatic scenarios. One can observe that Rdf, in both cases, is nearly normally distributed around zero with the main probability mass (99.5%) concentrated in the interval $[-2\%, 3\%]$. In addition, Rdf does not exceed in any case the interval $[-5\%, 10\%]$.

The estimation procedure for each experiment is very quick and takes 30 s in a typical personal PC with Intel®Core™ i5-5200CPU @2.20 GHz and 4.0 GB RAM.

Finally, one can argue that the present results may not seem in line with other published work in the climate community [17,49], where higher uncertainty levels are present. However, this is due to the fact that the present results are not directly comparable with the other aforementioned ones, because this simulation procedure analyses only the stochastic part (containing the correlation structure) and not the deterministic one (containing among others the long-term trends). Thus, the present methodology can be combined in the future with other existing tools, such as the dynamical models and/or other statistical models, to enhance the accuracy of the existing predictions of the wave climate by decreasing the computational cost, which in turn allows for finer computational grids.

3.2. Field-wise results

The same simulation procedure described in Section 3.1 is now applied to the whole field of points, shown in Fig. 2.

According to [35], since the remaining stationary W-part is almost homogeneous in space [50], only one datapoint is

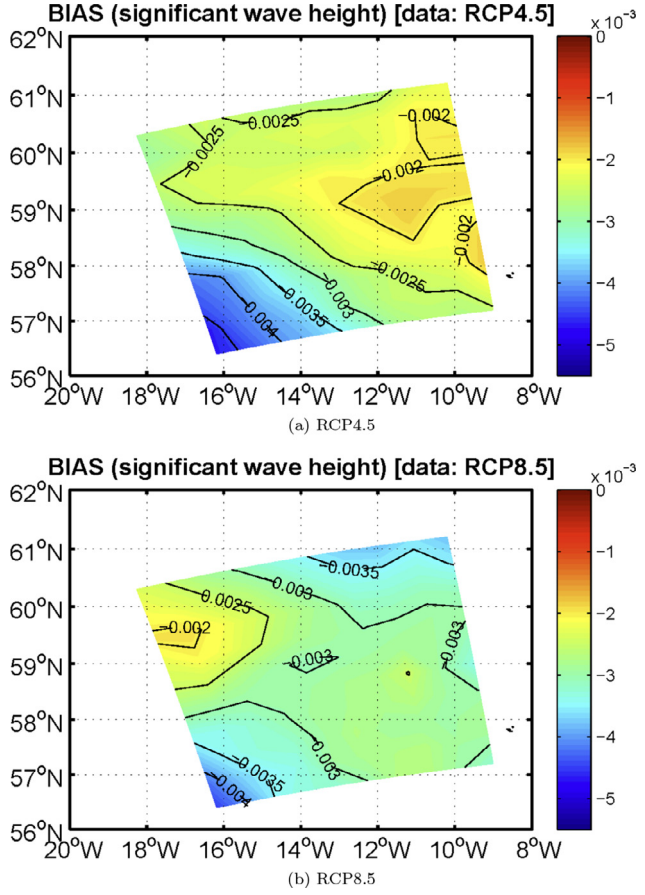

Fig. 15. Bias of the wave height estimates for Experiment 1 with respect to actual values for scenarios RCP4.5 and RCP8.5.

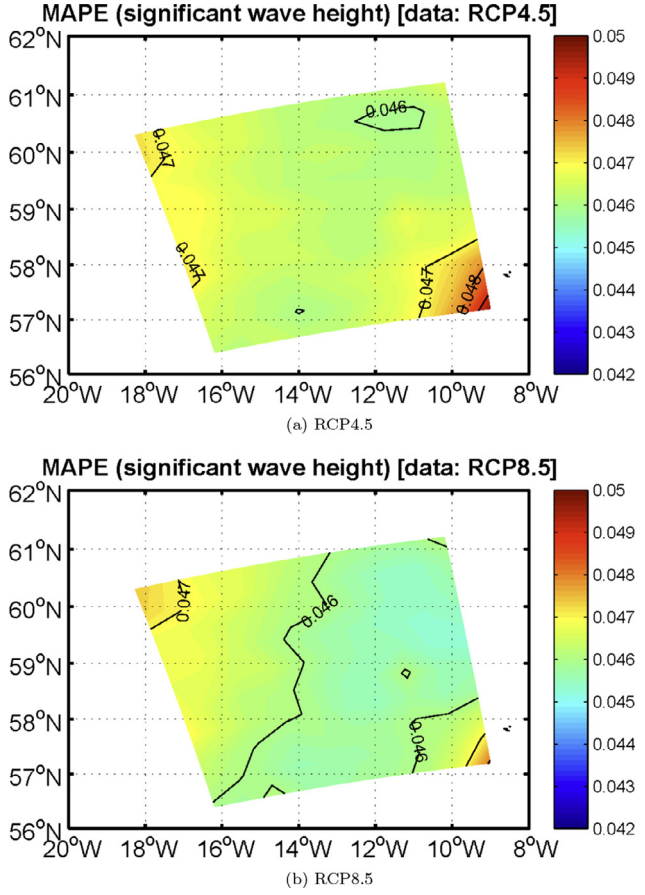

Fig. 16. MAPE of the wave height estimates for Experiment 1 with respect to actual values for scenarios RCP4.5 and RCP8.5.

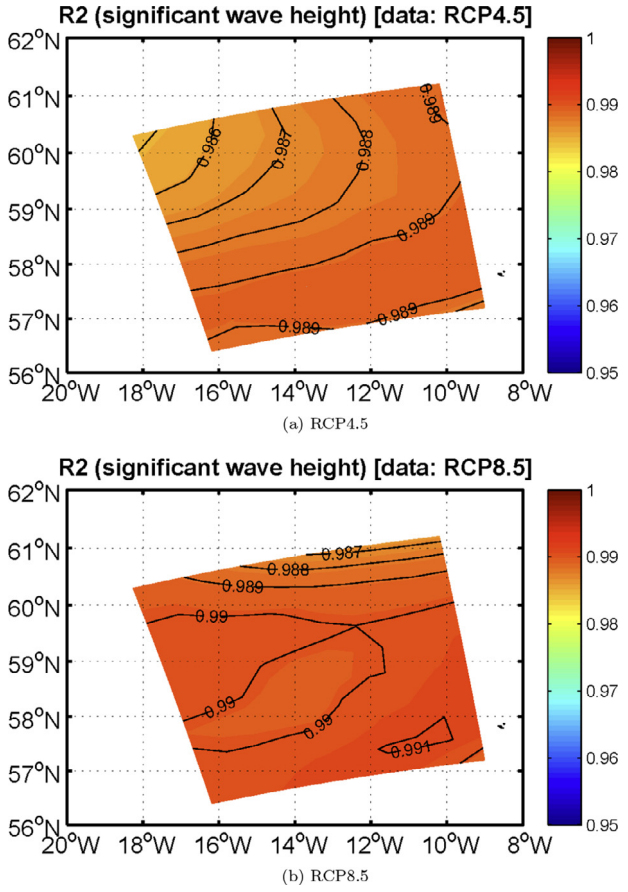

Fig. 17. R^2 of the wave height estimates for Experiment 1 with respect to actual values for scenarios RCP4.5 and RCP8.5.

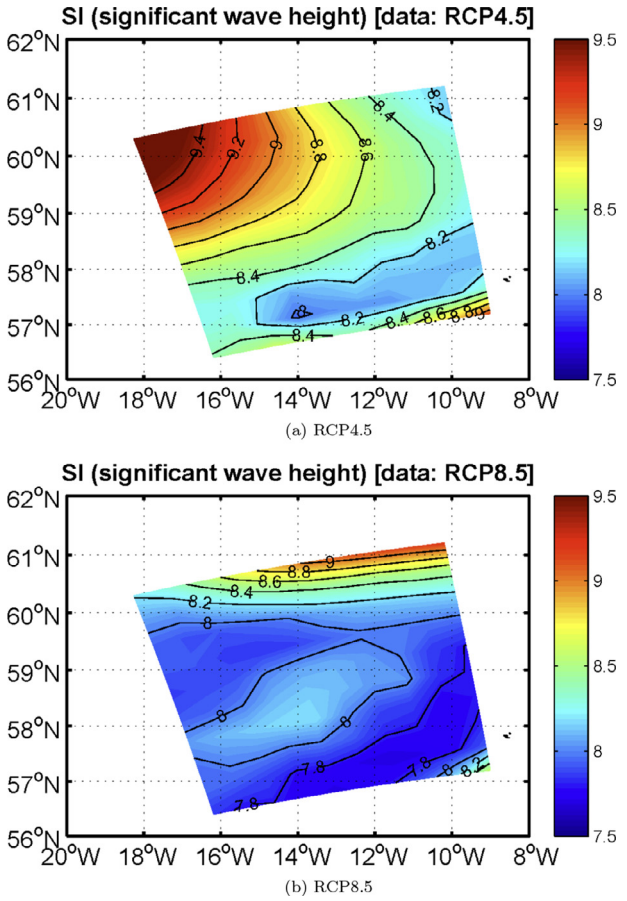

Fig. 18. SI of the wave height estimates for Experiment 1 with respect to actual values for scenarios RCP4.5 and RCP8.5.

needed for the fit of the FIS/ANFIS model; which greatly accelerates the calculations for the field forecasts.

Following the terminology of Section 3.1, W_1-series is taken from the point, already studied in Section 3.1, to estimate the parameters of the FIS/ANFIS model; see Fig. 2. Then, the estimated model is applied to the W_2-series of all other points of the field for the forecasting horizons of Experiments 1 and 2 given in Figs. 5 and 6.

Based on data kept for comparison purposes, all error measures described in Section 2.3 have been calculated. In Figs. 9–13 the error measures RMSE, Bias, MAPE, R^2 and SI for wind speed are depicted, while in Figs. 14–18 the same error measures are shown for significant wave height.

In those figures, one can observe that the root-mean-square error of the forecasts is less than 1.35 m/s for the wind speed and 0.3 m for the significant wave height. Also, the bias is very small (< -0.0035 m/s and < -0.002 m). The correlation coefficient is very high (95% for wind speed and 98–99%) for significant wave height). Finally, it is noteworthy that in most of the cases the spatial distribution of the various error measures is more or less uniform.

Furthermore, in order to study the spatial distribution of the maximum values, the following quantity is calculated for each grid point:

$$\mathrm{MAXdf}_s = \frac{|\max(A) - \max(S)|}{\max(A)} \times 100, \tag{19}$$

where A is the actual value kept for comparison, S is the simulation of the experiments, and $s = 1, \ldots, 100$ is the index of the grid points. An example of the results is given in Fig. 19(a) and (b), where the quantity MAXdf for the significant wave height is plotted for the two climate scenarios. The larger part of the grid points has MAXdf-values between 0% and 4% of the actual value, whereas there is a small part with values between 6% and 10% of the actual value.

4. Concluding remarks

Climatic simulations of significant wave height and wind speed have been obtained for the first time, based on a newly introduced procedure [35,36], where predictions were given for shorter periods. According to this, the well-known Fuzzy Inference Systems (FIS) in combination with Adaptive Neuro-Fuzzy Inference Systems (ANFIS), coupled with nonstationary time series modelling, is applied to obtain the forecasts.

Two datasets have been used; namely NORA10 (1957–2014) and ExWaCli (1971–2000 and 2071–2100), covering an

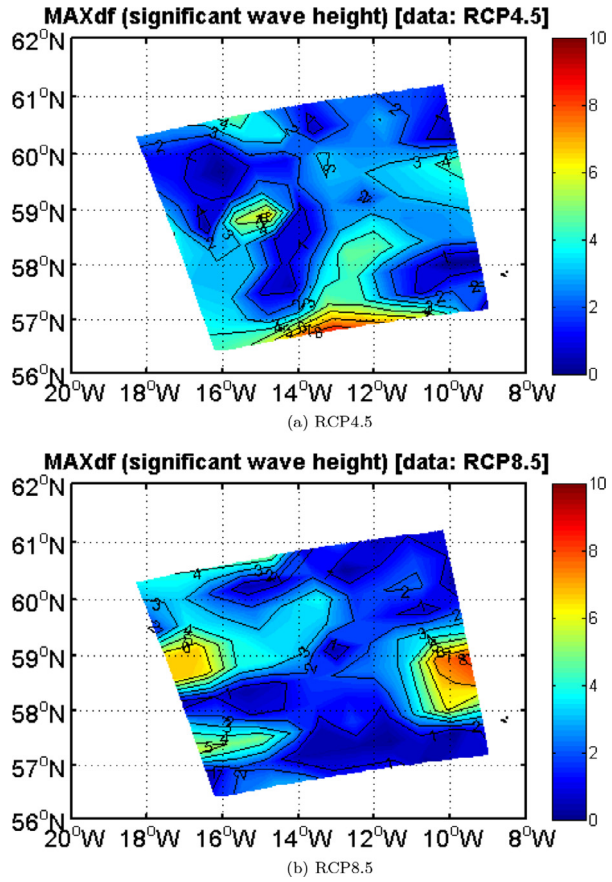

(a) RCP4.5

(b) RCP8.5

Fig. 19. MAXdf of the wave height estimates for Experiment 1 with respect to actual values for scenarios RCP4.5 and RCP8.5.

area of the North-eastern Atlantic Ocean, west of the British Isles, with partially overlapping computational grids.

Two forecasting experiments have been designed and performed. In the first one, the training set was the period 1957–1970 of the NORA10 dataset and the forecasts cover the periods 1971–2000 and 2071–2100. In the second one, the period 1971–2000 of ExWaCli dataset is the training set and the forecasts cover the periods 2001–2014 and 2071–2100.

The obtained forecasts are verified by means of actual values kept for comparison purposes. The calculated error measures show very good performance, demonstrating the feasibility of this methodology.

The present methodology makes it possible to explore the stochastic information contained in different datasets for different data periods to obtain simulated forecasts both in future and in past in climatic scales. In addition, the small amount of computational time needed makes it an attractive complementary tool in the process of obtaining future simulations in a climatic horizon, which is in line with the current demand of using enhanced computational tools [51].

Acknowledgements

This work has been partially funded by the RCN (Research Council of Norway) project “High-dimensional statistical modelling of changes in wave climate and implications for maritime infrastructure” (HDwave) under Contract No. 243814/E10, with partners Norsk Regnesentral (coordinator), DNV-GL and SINTEF Ocean.

The consortium of the project ExWaCli is thanked for the provision of NORA10 and ExWaCli datasets.

The authors wish also to thank anonymous reviewers for their fruitful comments that significantly improved the initial manuscript.

References

[1] IPCC, Fifth Assessment Report of the Intergovernmental Panel on Climate Change, Cambridge University Press, Cambridge, United Kingdom and New York, NY, USA, 2014, doi:10.1017/CBO9781107415324.

[2] The WAMDI Group, J. Phys. Oceanogr. 18 (12) (1988) 1775–1810, doi:10.1175/1520-0485(1988)018⟨1775:TWMTGO⟩2.0.CO;2.

[3] H. Tolman, J. Phys. Oceanogr. 21 (1991) 782–797, doi:10.1175/1520-0485(1992)022⟨1095:EONOTP⟩2.0.CO;2.

[4] D.P. Dee, S.M. Uppala, A.J. Simmons, P. Berrisford, P. Poli, S. Kobayashi, U. Andrae, M.A. Balmaseda, G. Balsamo, P. Bauer, P. Bechtold, A.C.M. Beljaars, L. van de Berg, J. Bidlot, N. Bormann, C. Delsol, R. Dragani, M. Fuentes, A.J. Geer, L. Haimberger, S.B. Healy, H. Hersbach, E.V. Hólm, L. Isaksen, P. Kållberg, M. Köhler, M. Matricardi, A.P. Mcnally, B.M. Monge-Sanz, J.J. Morcrette, B.K. Park, C. Peubey, P. de Rosnay, C. Tavolato, J.N. Thépaut, F. Vitart, Q. J. R. Meteorol. Soc. 137 (2011) 553–597, doi:10.1002/qj.828.

[5] A. Chawla, D.M. Spindler, H.L. Tolman, Ocean Model. 70 (2013) 189–206, doi:10.1016/j.ocemod.2012.07.005.

[6] B.G. Reguero, M. Menéndez, F.J. Méndez, R. Mínguez, I.J. Losada, Coast. Eng. 65 (2012) 38–55, doi:10.1016/j.coastaleng.2012.03.003.

[7] O.J. Aarnes, S. Abdalla, J.R. Bidlot, O. Breivik, J. Clim. 28 (2) (2015) 819–837, doi:10.1175/JCLI-D-14-00470.1.

[8] E. Vanem, Stoch. Environ. Res. Risk Assess. 25 (2011) 185–209, doi:10.1007/s00477-010-0431-y.

[9] F. Feser, M. Barcikowska, O. Krueger, F. Schenk, R. Weisse, L. Xia, Q. J. R. Meteorol. Soc. 141 (2015) 350–382, doi:10.1002/qj.2364.

[10] M. Reistad, O. Breivik, H. Haakenstad, O.J. Aarnes, B.R. Furevik, J.R. Bidlot, J. Geophys. Res.: Oceans 116 (5) (2011) 1–18, doi:10.1029/2010JC006402.

[11] O.J. Aarnes, M. Reistad, O. Breivik, E. Bitner-Gregersen, L.I. Eide, O. Gramstad, A.K. Magnusson, B. Natvig, E. Vanem, J. Geophys. Res.: Oceans 122 (2017) 3394–3403, doi:10.1002/2016JC012521.

[12] L.J. Donner, B.L. Wyman, R.S. Hemler, L.W. Horowitz, Y. Ming, M. Zhao, J.C. Golaz, P. Ginoux, S.J. Lin, M.D. Schwarzkopf, J. Austin, G. Alaka, W.F. Cooke, T.L. Delworth, S.M. Freidenreich, C.T. Gordon, S.M. Griffies, I.M. Held, W.J. Hurlin, S.A. Klein, T.R. Knutson, A.R. Langenhorst, H.C. Lee, Y. Lin, B.I. Magi, S.L. Malyshev, P.C.D. Milly, V. Naik, M.J. Nath, R. Pincus, J.J. Ploshay, V. Ramaswamy, C.J. Seman, E. Shevliakova, J.J. Sirutis, W.F. Stern, R.J. Stouffer, R.J. Wilson, M. Winton, A.T. Wittenberg, F. Zeng, J. Clim. 24 (13) (2011) 3484–3519, doi:10.1175/2011JCLI3955.1.

[13] R.H. Moss, J.A. Edmonds, K.A. Hibbard, M.R. Manning, S.K. Rose, D.P. van Vuuren, T.R. Carter, S. Emori, M. Kainuma, T. Kram, G.A. Meehl, J.F.B. Mitchell, N. Nakicenovic, K. Riahi, S.J. Smith, R.J. Stouffer, A.M. Thomson, J.P. Weyant, T.J. Wilbanks, Nature 463 (7282) (2010) 747–756, doi:10.1038/nature08823.

[14] D.P. van Vuuren, J. Edmonds, M. Kainuma, K. Riahi, A. Thomson, K. Hibbard, G.C. Hurtt, T. Kram, V. Krey, J.F. Lamarque, T. Masui, M. Meinshausen, N. Nakicenovic, S.J. Smith, S.K. Rose, Clim. Change 109 (1) (2011) 5, doi:10.1007/s10584-011-0148-z.

[15] R. de Winter, A. Sterl, B. Ruessink, J. Geophys. Res.: Atmos. 118 (2013) 1601–1612, doi:10.1002/jgrd.50147.

[16] X.L. Wang, Y. Feng, V.R. Swail, J. Geophys. Res.: Oceans 120 (2015) 3859–3871, doi:10.1002/2015JC010699.

[17] X.L. Wang, Y. Feng, V.R. Swail, Geophys. Res. Lett. 41 (3) (2014) 1026–1034, doi:10.1002/2013GL058650.
[18] I. Grabemann, N. Groll, Möller, R. Weisse, Ocean Dyn. 65 (2015) 255–267, doi:10.1007/s10236-014-0800-z.
[19] E. Vanem, E.M. Bitner-Gregersen, L.I. Eide, L. Garrè, P. Friis-Hansen, SNAME Trans. 122 (2015) 65–92.
[20] E. Vanem, J. Ocean Eng. Mar. Energy 1 (4) (2015) 339–359, doi:10.1007/s40722-015-0025-3.
[21] K.E. Taylor, R.J. Stouffer, G.A. Meehl, Bull. Am. Meteorol. Soc. 93 (4) (2012) 485–498, doi:10.1175/BAMS-D-11-00094.1.
[22] V. Eyring, S. Bony, G.A. Meehl, C.A. Senior, B. Stevens, R.J. Stouffer, K.E. Taylor, Geosci. Model Dev. 9 (2016) 1937–1958, doi:10.5194/gmd-9-1937-2016.
[23] M. Deo, A. Jha, A. Chaphekar, K. Ravikant, Ocean Eng. 28 (7) (2001) 889–898, doi:10.1016/S0029-8018(00)00027-5.
[24] S. Rao, S. Mandal, Ocean Eng. 32 (56) (2005) 667–684, doi:10.1016/j.oceaneng.2004.09.003.
[25] P. Jain, M. Deo, Appl. Ocean Res. 29 (12) (2007) 72–79, doi:10.1016/j.apor.2007.05.003.
[26] S. Mandal, N. Prabaharan, Ocean Eng. 33 (2006) 1401–1410, doi:10.1016/j.oceaneng.2005.08.007.
[27] N.K. Kumar, R. Savitha, A.A. Mamun, Ocean Eng. 129 (2017) 605–612, doi:10.1016/j.oceaneng.2016.10.033.
[28] M. Kazeminezhad, A. Etemad-Shahidi, S. Mousavi, Ocean Eng. 32 (1415) (2005) 1709–1725, doi:10.1016/j.oceaneng.2005.02.001.
[29] M. Özger, Z. Şen, Ocean Eng. 34 (3–4) (2007) 460–469, doi:10.1016/j.oceaneng.2006.03.003.
[30] J. Mahjoobi, A. Etemad-Shahidi, M. Kazeminezhad, Appl. Ocean Res. 30 (1) (2008) 28–36, doi:10.1016/j.apor.2008.03.002.
[31] A. Zamani, D. Solomatine, A. Azimian, A. Heemink, Ocean Eng. 35 (10) (2008) 953–962, doi:10.1016/j.oceaneng.2008.03.007.
[32] G. Sylaios, F. Bouchette, V.A. Tsihrintzis, C. Denamiel, Ocean Eng. 36 (1718) (2009) 1358–1365, doi:10.1016/j.oceaneng.2009.08.016.
[33] A. Akpinar, M. Özger, M.I. Kömörcü, J. Mar. Sci. Technol. 19 (1) (2014) 1–14, doi:10.1007/s00773-013-0226-1.
[34] Ch. Stefanakos, O. Schinas, WMU J. Marit. Aff. 14 (1) (2015) 177–199, doi:10.1007/s13437-015-0084-2.
[35] Ch. Stefanakos, Ocean Eng. 121 (2016a) 1–12, doi:10.1016/j.oceaneng.2016.05.018.
[36] Ch. Stefanakos, in: Proceedings of the Twenty-sixth International Offshore and Polar Engineering Conference, ISOPE'2016, International Society of Offshore & Polar Engineers, Rhodes (Rodos), Greece, 2016b, pp. 282–289.
[37] O. Duru, S. Yoshida, in: Proceedings of the 2012 IEEE Conference on Computational Intelligence for Financial Engineering & Economics (CIFEr), New York, 2012, pp. 1–7, doi:10.1109/CIFEr.2012.6327767.
[38] G. Athanassoulis, Ch. Stefanakos, J. Geophys. Res. Sec. Oceans 100 (C8) (1995) 16149–16162, doi:10.1029/94JC01022.
[39] Ch. Stefanakos, O. Schinas, Transp. Res. Part C: Emerg. Technol. 38 (1) (2014) 177–194, doi:10.1016/j.trc.2013.11.017.
[40] Ch. Stefanakos, E. Vanem, in: Proceedings of the Thirty-seventh International Conference on Ocean, Offshore and Arctic Engineering OMAE'2017, Trondheim, Norway, 2017.
[41] O.J. Aarnes, O. Breivik, M. Reistad, J. Clim. 25 (5) (2012) 1529–1543, doi:10.1175/JCLI-D-11-00132.1.
[42] P. Undén, Coauthors, Tech. Rep. Technical Report, S-601 76, 2002.
[43] E.M. Bitner-Gregersen, E. Vanem, O. Gramstad, T. Hørte, O.J. Aarnes, M. Reistad, O. Breivik, A.K. Magnusson, B. Natvig, Ocean Eng. 149 (2018) 226–237, doi:10.1016/j.oceaneng.2017.12.023.
[44] B.R. Furevik, H. Haakenstad, J. Geophys. Res.: Atmos. 117 (D23) (2012), doi:10.1029/2012JD018523. 14pp., d23106
[45] K. Bruserud, S. Haver, Ocean Dyn. 66 (6) (2016) 823–838, doi:10.1007/s10236-016-0953-z.
[46] A.P. Orimolade, S. Haver, O.T. Gudmestad, Mar. Struct. 49 (2016) 1–17, doi:10.1016/j.marstruc.2016.05.004.
[47] E. Vanem, Ocean Dyn. 64 (6) (2014) 879–893, doi:10.1007/s10236-014-0729-2.
[48] Ch. Stefanakos, G. Athanassoulis, S. Barstow, J. Geophys. Res. Sec. Oceans 111 (C10) (2006) 10001–10012, doi:10.1029/2005JC003020.
[49] M. Dobrynin, J. Murawsky, S. Yang, Geophys. Res. Lett. 39(18). 10.1029/2012GL052843
[50] Ch. Stefanakos, Proc. Inst. Mech. Eng. Part M: J. Eng. Marit. Environ. 222 (2008) 27–39, doi:10.1243/14750902JEME64.
[51] J. Shukla, T.N. Palmer, R. Hagedorn, B. Hoskins, J. Kinter, J. Marotzke, M. Miller, J. Slingo, Bull. Am. Meteorol. Soc. 91 (10) (2010) 1407–1412, doi:10.1175/2010BAMS2900.1.